



Cite this: *Nanoscale Horiz.*, 2024, 9, 843

Received 4th December 2023,  
Accepted 5th March 2024

DOI: 10.1039/d3nh00541k

rsc.li/nanoscale-horizons

## Universal nanocomposite coating with antifouling and redox capabilities for electrochemical affinity biosensing in complex biological fluids†

Aditya Manu Bharti,<sup>‡</sup> R. K. Rakesh Kumar,<sup>‡</sup> Cheng-Hsin Chuang<sup>\*,be</sup> and Muhammad Omar Shaikh<sup>\*,f</sup>

Electrochemical affinity biosensors have the potential to facilitate the development of multiplexed point-of-care diagnostics in complex biological fluids. However, their commercial viability has been hindered by challenges such as electrode biofouling and the lack of inherent redox properties. To address this unmet need, we have developed a universal nanocomposite coating which is unique in its ability to not only allow oriented conjugation of the biorecognition element but also specific detection directly in complex biological fluids like serum and urine owing to its built-in antifouling and redox capabilities, thus improving suitability for point of care testing. This multifunctional coating comprises a 3D porous crosslinked bovine serum albumin matrix for oriented conjugation and antifouling properties with embedded graphene nanosheets modified with amino-ferrocene for enhanced conductivity and mediator-free biosensing. The coating showed minimal signal degradation despite prolonged exposure to 1% bovine serum albumin, artificial urine and untreated human serum for up to 30 days. To demonstrate its utility, we fabricated and tested proof-of-concept electrochemical immunosensors for bladder cancer protein biomarkers, specifically interleukin-8 (IL-8) and vascular endothelial growth factor (VEGF). The practical feasibility was highlighted by the excellent sensitivity and specificity observed for IL-8 and VEGF with a limit of detection of 41 pg mL<sup>-1</sup> and 67 pg mL<sup>-1</sup>, respectively. Consequently, this universal nanocomposite-based electrochemical biosensing platform can be extended to the point of care testing of a broad spectrum of biomarkers present in complex biological fluids, thus enabling reliable and early diagnostics.

### New concepts

While electrochemical biosensors hold promise for enabling the development of multiplexed point-of-care diagnostics, their commercial viability has been hindered by challenges such as electrode biofouling and the absence of inherent redox properties. In this study, we have successfully developed a novel and universal 3D nanocomposite electrode coating which is designed to specifically tackle three important challenges in electrochemical immunosensing: (i) improved antibody immobilization, (ii) antifouling properties, and (iii) mediator-free sensing capability. This multifunctional coating will be the first of its kind to not only allow oriented antibody immobilization but also specific detection directly in complex fluids like urine and serum owing to its in-built antifouling and redox capabilities, thus improving suitability for point-of-care testing. To demonstrate its practical utility, we fabricated and tested proof-of-concept electrochemical immunosensors for bladder cancer protein biomarkers IL-8 and VEGF which demonstrated excellent sensitivity and specificity with a limit of detection of 41 pg mL<sup>-1</sup> and 67 pg mL<sup>-1</sup>, respectively. The proposed universal nanocomposite-based electrochemical biosensing platform can be extended to the point of care testing of a broad spectrum of biomarkers present in complex biological fluids, thus enabling reliable and early diagnostics of a wide range of medical conditions.

## 1. Introduction

Electrochemical affinity biosensors represent a remarkable fusion of the exceptional specificity of affinity biorecognition and the convenience, cost-effectiveness, reasonable sensitivity, and adaptability of electrochemical transduction, making them

<sup>a</sup> International PhD Program for Science, National Sun Yat-sen University, Kaohsiung 80424, Taiwan

<sup>b</sup> Institute of Medical Science and Technology, National Sun Yat-sen University, Kaohsiung 80424, Taiwan. E-mail: chchuang@imst.nsysu.edu.tw; Tel: +886-75-252-000 ext. 7151

<sup>c</sup> Department of Chemical Engineering, National Taiwan University, Taipei City, 10617, Taiwan

<sup>d</sup> Institute of Biomedical Engineering and Nanomedicine, National Healthcare Research Institutes, Miaoli County 350, Taiwan

<sup>e</sup> Centre of Excellence for Metabolic Associated Fatty Liver Disease (CEMAFLD), National Sun Yat-sen University, Kaohsiung 80424, Taiwan

<sup>f</sup> Sustainability Science and Management Program, Tunghai University, Taichung 407224, Taiwan. E-mail: omar@thu.edu.tw; Tel: +886-4-23590121 ext.39204

† Electronic supplementary information (ESI) available. See DOI: <https://doi.org/10.1039/d3nh00541k>

‡ Aditya Manu Bharti and R. K. Rakesh Kumar have equally contributed to this work.

highly suitable for seamless integration with compact electronic devices.<sup>1–3</sup> Consequently, these biosensors offer an ideal solution for developing cost-effective multiplexed diagnostic technologies that can precisely detect specific analytes in complex biological fluids, such as urine and serum.<sup>4–6</sup> Nevertheless, the current feasibility of electrochemical biosensors for point-of-care testing (POCT) is significantly restricted due to several key challenges: (i) limited performance: the inefficiency in conjugation of biorecognition elements results in suboptimal sensitivity and specificity<sup>7,8</sup>; (ii) biofouling: uncontrolled biofouling inevitably deteriorates the electrode morphology, leading to a rapid loss in sensitivity<sup>9,10</sup>; (iii) lack of built-in redox properties: the absence of intrinsic redox capability necessitates the use of additional steps and external redox-probes.<sup>11,12</sup> These limitations result in a scarcity of studies reporting on electrochemical affinity biosensors capable of performing direct detection in unprocessed biofluids.<sup>13,14</sup> Consequently, these traditional biosensors are plagued by non-specificity and reduced sensitivity, making them highly susceptible to external factors and thereby restricting their commercial viability.<sup>15,16</sup>

Typically, affinity biorecognition elements, including antibodies, aptamers, and nucleic acids are anchored to the electrode surface through physical adsorption *via* weak Van-der Waals forces, entrapment in solid media such as gels, electrostatic interactions, or covalent binding.<sup>17–24</sup> Among these methods, covalent linkage provides the strongest conjugation and is considered the most ideal approach.<sup>25</sup> It is crucial to note that the spatial configuration of the biorecognition element significantly influences the biorecognition event.<sup>26</sup> Currently available electrochemical biosensors often face sensitivity and specificity constraints due to the limited availability of active sites with proper orientations for effective biorecognition. Additionally, non-specific interactions with interferents, especially proteins, present in the sample fluids pose a significant risk of producing false-positive results. The issue of biofouling in traditional electrochemical biosensors, coupled with the absence of built-in redox mediators, limits their ability to perform sensitive and specific detection directly in complex biological fluids.<sup>27,28</sup> To tackle this issue, numerous recent studies have been conducted to enable antifouling capabilities through the integration of polymers and hydrogels with the electrode surface.<sup>29,30</sup> However, such approaches still rely on the utilization of external redox probes which requires extra washing and detection steps, thus complicating the process and reducing practical applicability for POCT.<sup>31,32</sup> Moreover, the prevalence of diseases with characteristic asymptomatic early stages and high end-stage mortality, such as chronic disorders and cancer, underscores the urgent need for multiplexed point-of-care diagnostics.<sup>33,34</sup> Therefore, the development of a universal electrode coating with integrated functionalities such as improved immobilization of biorecognition elements, excellent antifouling behaviour and built-in redox capability is pivotal for the successful commercialization of multiplexed electrochemical affinity biosensors.<sup>35</sup>

Herein, we have addressed this unmet need and developed a universal nanocomposite coating for electrochemical affinity biosensing in complex biological fluids. This coating utilizes a

3D porous matrix of crosslinked bovine serum albumin (BSA) embedded with graphene nanosheets functionalized with amino-ferrocene (Fc-GNS). The components and functionalities of this nanocomposite coating include: (i) 3D BSA matrix, which facilitates oriented covalent conjugation of the biorecognition element, eliminates biofouling, and allows analyte diffusion through its pores without hindrance. (ii) Embedded Fc-GNS for improved conductivity and mediator-free biosensing directly in complex biological fluids. Our developed nanocomposite coating demonstrated exceptional antifouling behaviour even after a month-long incubation in 1% BSA, artificial urine and untreated human serum. For proof-of-concept feasibility studies, we utilized the nanocomposite coating modified electrodes for electrochemical immunosensing of two bladder cancer protein biomarkers, namely interleukin-8 (IL-8) and vascular endothelial growth factor (VEGF). The respective antibodies were successfully immobilized using ethylene dichloride (EDC) and *N*-hydroxysuccinimide (NHS) chemistry which efficiently forms a carbodiimide bond between the carboxylic groups of aspartate and glutamate side chains in the BSA matrix and the amine groups in the antibodies. The electrochemical immunosensors achieved an impressive limit of detection (LOD) of 41 pg mL<sup>-1</sup> for IL-8 and 67 pg mL<sup>-1</sup> for VEGF, respectively, broad sensing range of 0.1 to 1000 ng mL<sup>-1</sup> for both biomarkers and high specificity against other protein interferents such as NMP-22, FGFR3, and HSA. To the best of our knowledge, this multifunctional nanocomposite coating is the first of its kind to not only allow oriented immobilization of the biorecognition element but also enable specific detection directly in complex biological fluids owing to its intrinsic antifouling and mediator-free capabilities. This universal coating shows promise in facilitating multiplexed electrochemical biosensing of a broad spectrum of biomarkers present in biological fluids, thus enabling reliable POCT of a wide range of medical conditions.

## 2. Materials and methods

### 2.1. Materials

Graphene nanosheets (GNS, <3 nm), amino-ferrocene (Fc-NH<sub>2</sub>, >98%), sodium hydroxide (NaOH, >97%), sulfuric acid (H<sub>2</sub>SO<sub>4</sub>), hydrochloric acid (HCl), 2-(*N*-morpholino) ethanesulfonic acid buffer (MES hydrate, ≥99.5%), *N*-ethyl-*N'*-(3-dimethylamino-propyl) carbodiimide hydrochloride (EDC, C<sub>8</sub>H<sub>17</sub>N<sub>3</sub>·HCl, ≥99.0%), glutaraldehyde (GA, OHC(CH<sub>2</sub>)<sub>3</sub>CHO, 25% in H<sub>2</sub>O), potassium hexacyanoferrate(II) trihydrate (K<sub>4</sub>Fe(CN)<sub>6</sub>·3H<sub>2</sub>O, 98.5–102.0%) and potassium hexacyanoferrate(III) (K<sub>3</sub>Fe(CN)<sub>6</sub>, ≥99.0%) were purchased from Sigma-Aldrich. *N*-Hydroxysuccinimide (NHS, C<sub>4</sub>H<sub>5</sub>NO<sub>3</sub>, >98%), bovine serum albumin (BSA) and artificial human urine were purchased from Fisher Scientific. Monoclonal antibodies for interleukin-8 (IL-8) and vascular endothelial growth factor (VEGF), as well as proteins for IL-8, VEGF, fibroblast growth factor receptor-3 (FGFR3), nuclear matrix protein-22 (NMP22), and human serum albumin (HSA), were purchased from Abcam. All solutions were prepared

using deionized water with a resistivity of 18.2 M $\Omega$ , unless otherwise stated.

## 2.2. Instrumentation

We employed a variety of microscopy techniques to analyze the nanocomposite-modified electrode. Field emission scanning electron microscopy (FESEM, JEOL JSM-6330) and atomic force microscopy (AFM, Seiko SPA 300-HV) were utilized to examine the structure and surface characteristics. To ensure the uniform distribution of ferrocene on the graphene surface and perform elemental mapping of the synthesized Fc-GNS through energy dispersive spectrometry, we used a field emission gun transmission electron microscope (FEG-TEM, Tecnai G2 F30 S-TWIN). Additionally, we conducted chemical analysis of Fc-GNS using attenuated total reflectance Fourier transform infrared spectroscopy (ATR-FTIR, Thermo Scientific Nicolet iS5) and high-resolution X-ray photoelectron spectroscopy (XPS, JEOL JPS 9030). For our electrochemical investigations, we employed an electrochemical workstation (Autolab PGSTAT204). The electrochemical setup was configured as a three-electrode system, with the working electrode consisting of a screen-printed carbon electrode (SPCE), the counter electrode being a platinum wire, and the reference electrode as Ag/AgCl in a 3 M KCl solution.

## 2.3. Synthesis of Fc-GNS

Graphene nanosheets (GNS) were subjected to a treatment involving a combination of HCl and H<sub>2</sub>SO<sub>4</sub> in a 3:1 ratio to introduce carboxylic groups. Following this modification, the GNS were thoroughly rinsed with deionized water and subsequently subjected to vacuum drying. Subsequently, 20 mg of the dried modified GNS (referred to as M-GNS) were dissolved in a 10 mL solution containing EDC/NHS, which had been prepared in MES buffer at a pH of 6.1. This mixture was prepared using a 2:1 ratio of EDC to NHS, respectively. The M-GNS solution was then subjected to sonication for a duration of 30 minutes and subsequently centrifuged to remove any excess reagents. Concurrently, another solution was prepared by mixing 20 mg of aminoferrocene (Fc-NH<sub>2</sub>) with MES buffer at a pH of 6.1. Subsequently, the M-GNS were introduced into this solution to facilitate the covalent functionalization of GNS with Fc, resulting in the formation of Fc-GNS. This reaction took place at room temperature and continued for a duration of 6 hours. The resulting Fc-GNS sheets underwent multiple rounds of washing with deionized water until the supernatant became colorless. The collected Fc-GNS were redispersed in DI water and stored at 4 °C for later use.

## 2.4. Synthesis of Fc-GNS/BSA/GA nanocomposite

The synthesis of the optimized Fc-GNS/BSA/GA nanocomposite involved the mixing of Fc-GNS (68  $\mu$ L, 20 mg mL<sup>-1</sup>) and BSA (68  $\mu$ L, 7.5 mg mL<sup>-1</sup>) solutions, followed by the addition of 2  $\mu$ L of GA. The introduction of GA initiated the protein crosslinking reactions, resulting in the formation of a nanocomposite where Fc-GNS was embedded within the crosslinked 3D BSA matrix. To synthesize the optimized nanocomposite, we initially explored different volumes of GA to crosslink the BSA, as illustrated in

Table 1 Optimization using different volumes of GA to crosslink the BSA

Sample name	Volume of 7.5 mg mL <sup>-1</sup> BSA ( $\mu$ L)	Volume of 25% GA ( $\mu$ L)	Total volume ( $\mu$ L)
BSA/GA-0	70	0	70
BSA/GA-1	69	1	70
BSA/GA-2	68	2	70
BSA/GA-3	67	3	70

Table 1, and subsequently investigated different BSA/Fc-GNS concentration ratios, as depicted in Table 2.

## 2.5. Development of immunosensors

**2.5.1. Characterization of the optimized nanocomposite coating.** The characterization of the optimized 3D Fc-GNS/BSA/GA nanocomposite coating was determined through two methods: morphological characterization using SEM and electrochemical characterization using cyclic voltammetry (CV). Initially, we conducted optimization studies by varying the volume of GA for crosslinking BSA (as shown in Table 1). The BSA/GA mixture was drop-casted onto the SPCE and allowed to dry at 37 °C for 6 hours. Subsequently, we examined the resulting morphology using SEM to assess the porosity and uniformity of the coating, and the degree of crosslinking. We also investigated the electrochemical charge transfer behavior using CV in a 5 mM Fe(CN<sub>6</sub>)<sup>-3</sup>/Fe(CN<sub>6</sub>)<sup>-4</sup> solution. To facilitate mediator-free electrochemical biosensing, we utilized the optimized BSA/GA volume and conducted further studies, this time varying the Fc-GNS/BSA concentration ratios (as shown in Table 2). Finally, the optimized Fc-GNS/BSA/GA nanocomposite coating was drop-casted onto the SPCE and dried at 37 °C for 6 hours. SEM was utilized to analyze the morphology of both the bare SPCE and SPCE/Fc-GNS/BSA/GA. Lastly, we studied the electrochemical charge transfer behavior and scan rate dependencies through CV in a 0.2 M PBS solution. The voltammograms obtained at various scan rates provided valuable insights into the electron transfer dynamics and redox characteristics of the nanocomposite modified electrode.

**2.5.2. Anti-fouling performance of the nanocomposite coating.** The efficacy of the nanocomposite coating in preventing biofouling was assessed using differential pulse voltammetry (DPV). The nanocomposite modified SPCE was immersed in diverse complex fluids, such as 1% BSA, artificial urine and untreated human serum, for varying timeframes, including 1 hour, 1 day, 1 week, and 1 month. The degree of reduction in peak current magnitude, observed after extended exposure to these complex fluids in comparison to the initial peak current of fresh coatings, served as a dependable indicator of the antifouling properties of the nanocomposite coating. Additionally, a control experiment was conducted with a bare SPCE, which was also immersed in artificial urine for the same durations, to validate the occurrence of biofouling in the absence of the nanocomposite coating.

**2.5.3. Fabrication and feasibility of immunosensors.** To highlight the practical applicability of the nanocomposite coating, we developed two proof-of-concept electrochemical

Table 2 Optimization using different BSA/Fc-GNS concentration ratios

Sample	Concentration of BSA (mg mL <sup>-1</sup> )	Volume of 25% GA (μL)	Concentration of Fc-GNS (mg mL <sup>-1</sup> )	BSA/Fc-GNS concentration ratio
Fc-GNS-5/BSA/GA-2	7.5	2	5	1.5
Fc-GNS-10/BSA/GA-2	7.5	2	10	0.75
Fc-GNS-20/BSA/GA-2	7.5	2	20	0.375
Fc-GNS-30/BSA/GA-2	7.5	2	30	0.25

immunosensors for detection of bladder cancer protein biomarkers, specifically interleukin-8 (IL-8) and vascular endothelial growth factor (VEGF). The systematic protocol for the fabrication of the immunosensors, which involves the synthesis of the Fc-GNS, 3D nanocomposite preparation, modification of the electrode, and operation of the immunosensor using DPV, is schematically presented in Fig. 1. Initially, the Fc-GNS/BSA/GA nanocomposite was prepared by combining 68 μL of BSA (7.5 mg mL<sup>-1</sup>) and 68 μL of Fc-GNS (20 mg mL<sup>-1</sup>) through vortex mixing followed by the addition of 2 μL of 25% GA to initiate the crosslinking process. Subsequently, 15 μL of the nanocomposite was drop-cast onto the electrode and then dried in an incubator at 37 °C for 6 hours. Following the drying process, the antibody (IL-8 or VEGF) was immobilized to the BSA matrix using EDC/NHS chemistry. Briefly, the nanocomposite modified electrodes underwent a 30-minute treatment with EDC/NHS, followed by rinsing with DI water. After drying at room temperature, 15 μL of antibody (at a concentration of 300 μg mL<sup>-1</sup>, with 0.5% glycerol in PBS at pH 7.4) was incubated and held for 1 hour at 4 °C. Following antibody conjugation, the electrodes were rinsed with a solution consisting of 1% BSA and 0.05% Tween-20 in a 0.2 M PBS solution and then allowed to dry. This modified electrode, composed of SPCE/Fc-GNS/BSA/GA/antibody, can be readily employed for immunosensing or stored at 4 °C for future use.

The feasibility of the fabricated proof-of-concept immunosensors was assessed by testing them in artificial urine that had

been spiked with the antigen (IL-8 or VEGF). DPV measurements were carried out within a potential range of -0.2 to 0.9 V (with a step of 0.003 V and a scan rate of 0.006 V s<sup>-1</sup>) using the SPCE/Fc-GNS/BSA/GA/Antibody as the working electrode, Ag/AgCl as the reference electrode, and Pt as the counter electrode. The peak current value obtained after immobilizing the antibody was denoted as “I<sub>0</sub>.” Subsequently, immunosensing was performed in artificial urine spiked with different antigen concentrations: 0.1 ng mL<sup>-1</sup>, 1 ng mL<sup>-1</sup>, 10 ng mL<sup>-1</sup>, 100 ng mL<sup>-1</sup>, and 1000 ng mL<sup>-1</sup>. DPV measurements were conducted after immunosensing, and the resulting peak current values were noted as “I.” The quantification of the immunosensor response was achieved by normalizing the change in peak current during immunosensing with the peak current observed after antibody immobilization. The utilization of a normalized immunosensor response serves to mitigate any variations arising from the initial resistance of individual electrodes. Subsequently, the immunosensor response to varying concentrations of the antigen was employed to establish a calibration curve, facilitating the determination of sensitivity and LOD. To ensure the reliability and consistency of the results, five separate immunosensors were assessed for each concentration of the antigen. Finally, specificity tests were carried out in the presence of interfering proteins that could potentially exist in urine. These tests were conducted in artificial urine spiked with 1 μg mL<sup>-1</sup> of NMP-22, HSA, and FGFR3, and the resulting immunosensor responses were compared.

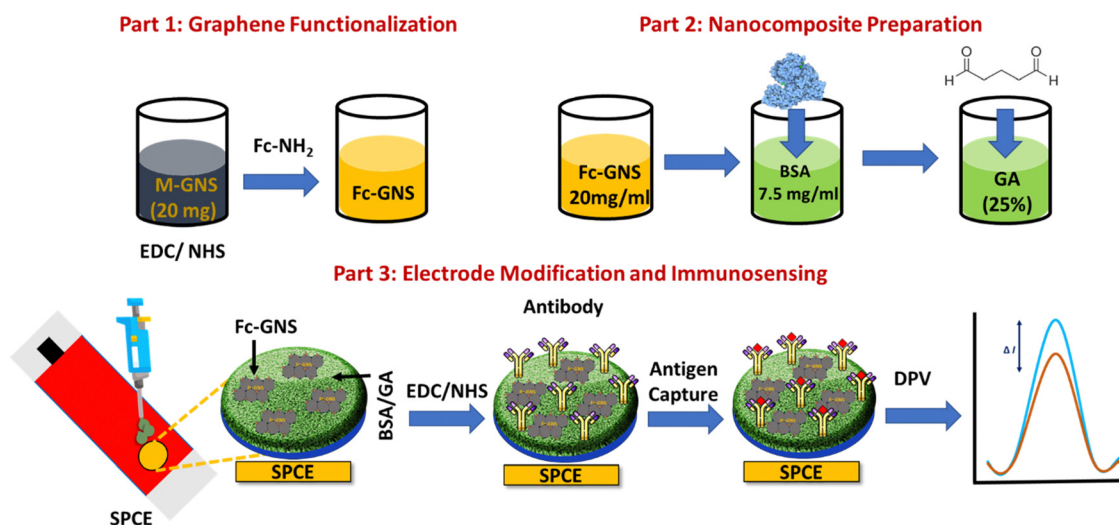


Fig. 1 Schematic illustration depicting the step-by-step procedure for the synthesis of Fc-GNS and the 3D nanocomposite, electrode modification, and immunosensing using DPV.

### 3. Results and discussion

#### 3.1. Characterization of Fc-GNS

Morphological and chemical characterizations of Fc-GNS were performed using TEM, EDS, ATR-FTIR, and XPS, as depicted in Fig. 2. The TEM analysis revealed a uniform deposition of ferrocene on the surface of GNS, which was substantiated by the detection of elemental Fe in the EDS mapping. ATR-FTIR analysis was conducted to compare the Fc-GNS-coated SPCE with both the bare and M-GNS-coated SPCE. Equal amounts of M-GNS and Fc-GNS were dissolved in DI water and 15  $\mu\text{L}$  was dropped on the SPCE. In the absence of any coatings, the bare SPCE exhibited a transmittance peak at 2300  $\text{cm}^{-1}$ , which was attributed to the presence of carbon-carbon double bonds (C=C).

The M-GNS-coated SPCE displayed a peak at 2300  $\text{cm}^{-1}$  (C=C) and an additional peak at 1000  $\text{cm}^{-1}$ , corresponding to C-O stretching vibrations. This indicated the presence of various COOH groups on the graphene surface.<sup>36</sup> The Fc-GNS-coated SPCE exhibited transmittance peaks at 3350  $\text{cm}^{-1}$  (N-H), 2300  $\text{cm}^{-1}$  (C=C), 1000  $\text{cm}^{-1}$  (OH), and 1500  $\text{cm}^{-1}$  (C-N).<sup>37</sup> The emergence of peaks around 1500  $\text{cm}^{-1}$ , associated with C-N stretching vibrations, and a significant reduction in peaks at 1000  $\text{cm}^{-1}$ , indicative of the involvement of COOH groups, confirmed the presence of an amide bond formed between the COOH group of M-GNS and the  $\text{NH}_2$  group of aminoferrocene, affirming the successful synthesis of Fc-GNS. Furthermore, the XPS spectra of Fc-GNS displayed characteristic peaks corresponding to the binding energies of C1s (286 eV),<sup>38</sup> O1s

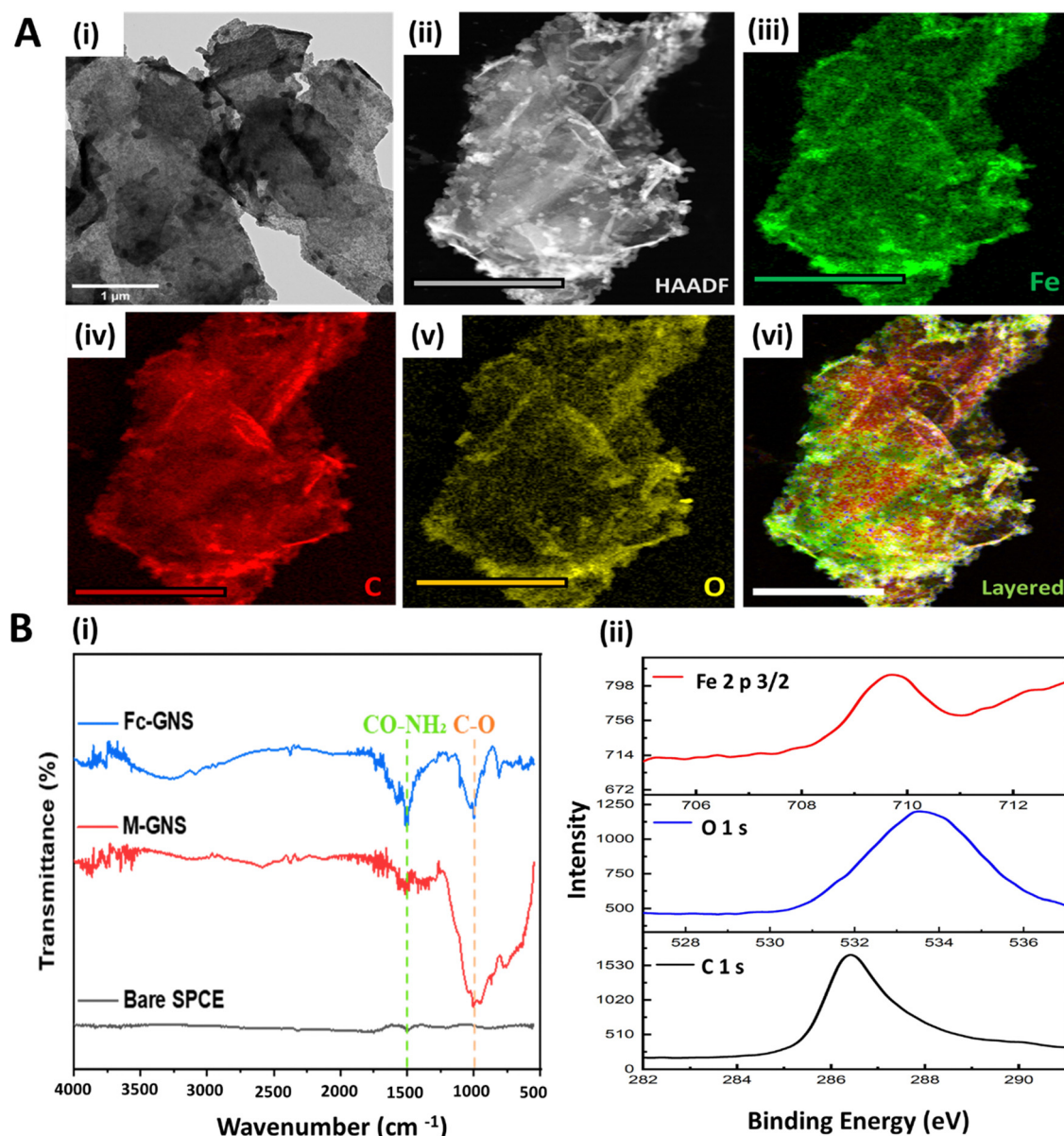


Fig. 2 (A) (i) TEM and (ii) HAADF image of Fc-GNS. EDS elemental map showing the presence of (iii) Fe, (iv) C, (v) O and (vi) layered map of Fc-GNS. [Scale bar = 5  $\mu\text{m}$ ]. (B) (i) FTIR spectra of bare SPCE, M-GNS coated SPCE and Fc-GNS coated SPCE (B ii) XPS spectra of Fc-GNS.

(534 eV),<sup>39</sup> and Fe 2p<sub>3/2</sub> (710 eV).<sup>40,41</sup> These peaks confirmed the presence of constituent elements and their chemical states in Fc-GNS.<sup>42</sup>

### 3.2. Morphological characterization of the nanocomposite coating

The optimized Fc-GNS/BSA/GA nanocomposite was prepared by first investigating various volumes of GA used for crosslinking BSA. The surface of the modified electrodes, where BSA was crosslinked using varying volumes of GA (referred to as BSA/GA-0, BSA/GA-1, BSA/GA-2, and BSA/GA-3), was examined using SEM, as shown in Fig. 3A. A comparison of these modified electrodes revealed significant changes in their morphology, influencing their overall porosity and roughness. Notably, BSA/GA-0, which did not include any GA, exhibited a smooth surface devoid of any porosity. BSA/GA-1, which contained a smaller amount of GA (1  $\mu$ L), also displayed a relatively smooth surface, mainly due to the limited crosslinking. In contrast, BSA/GA-2 and BSA/GA-3 displayed rough and porous surfaces. Based on the SEM images, it was expected that BSA/GA-2 and BSA/GA-3, with their high porosity and roughness, would exhibit superior electrochemical properties compared to BSA/GA-0 and BSA/GA-1, which had smoother surfaces. Detailed electrochemical testing revealed that BSA/GA-2 exhibited the highest peak current, which is further discussed in the subsequent section. Consequently, BSA/GA-2 was utilized to synthesize the optimized Fc-GNS/BSA/GA nanocomposite, demonstrating a morphology that significantly differed from the bare SPCE, as depicted in Fig. 3B. Moreover, the surface roughness and topography of the optimized nanocomposite coating were examined using AFM, revealing that the coating surface exhibited roughness, with a maximum height variation of 500 nm.

### 3.3. Electrochemical characterization of the nanocomposite coating

Based on the morphology and extent of crosslinking in the BSA/GA coatings, it was anticipated that BSA/GA-2 and BSA/GA-3 would exhibit better electrochemical performance compared to BSA/GA-1. To investigate this hypothesis and identify the optimal conditions for producing the nanocomposite, CV was conducted in a 5 mM  $\text{Fe}(\text{CN})_6^{3-}/\text{Fe}(\text{CN})_6^{4-}$  solution to assess the electrochemical behavior and charge transfer capabilities. Our observations revealed that the SPCE modified with BSA/GA-2 exhibited the highest anodic current and improved charge transfer, surpassing both BSA/GA-1 and BSA/GA-3, as depicted in Fig. 4B(i and ii). BSA/GA-1, which contains a lower amount of GA, results in poor crosslinking and reduced porosity, while BSA/GA-3 leads to excessive crosslinking and a thicker coating, both of which impede charge transfer. Consequently, BSA/GA-2 was selected for further investigation due to its superior electrochemical performance.

In the subsequent phase, we sought to eliminate the requirement for an external redox mediator and enhance the conductive characteristics of the nanocomposite. To achieve this, we integrated varying quantities of Fc-GNS into the BSA/GA-2 matrix. Four distinct BSA/Fc-GNS concentration ratios, specifically 1.5, 0.75, 0.375, and 0.25, were employed, and their electrochemical behaviour and charge transfer properties were investigated through CV in a 0.2 M PBS solution, as depicted in Fig. 4B(iii and iv). It was worth noting that the bare SPCE displayed a weak electrochemical response in PBS, with no discernible redox properties and the absence of either cathodic or anodic current. However, the Fc-GNS/BSA/GA nanocomposite-modified SPCE exhibited redox properties, and notably, an upward trend was observed particularly in the anodic peak current, as the concentration of Fc-GNS was increased.

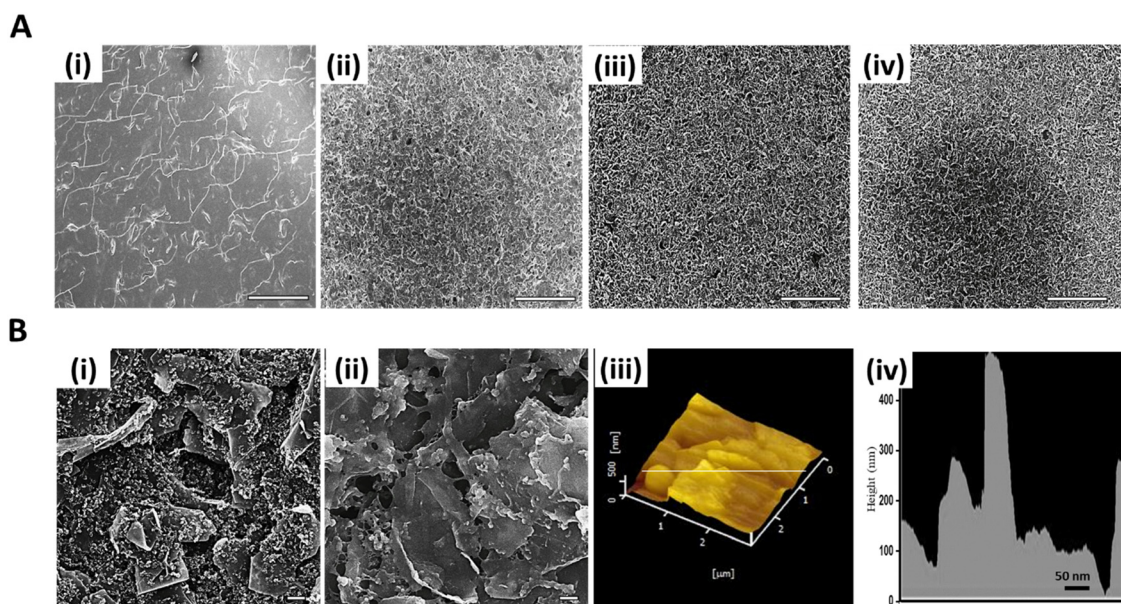


Fig. 3 (A) (i) SEM images of SPCE modified with (i) BSA/GA-0 (ii) BSA/GA-1 (iii) BSA/GA-2 and (iv) BSA/GA-3. [Scale bar = 100  $\mu$ m]. (B) SEM images of (i) Bare SPCE and (ii) SPCE/Fc-GNS/BSA/GA [Scale bar = 1  $\mu$ m]. AFM topography of (iii) SPCE/Fc-GNS/BSA/GA and (iv) an extracted height profile.

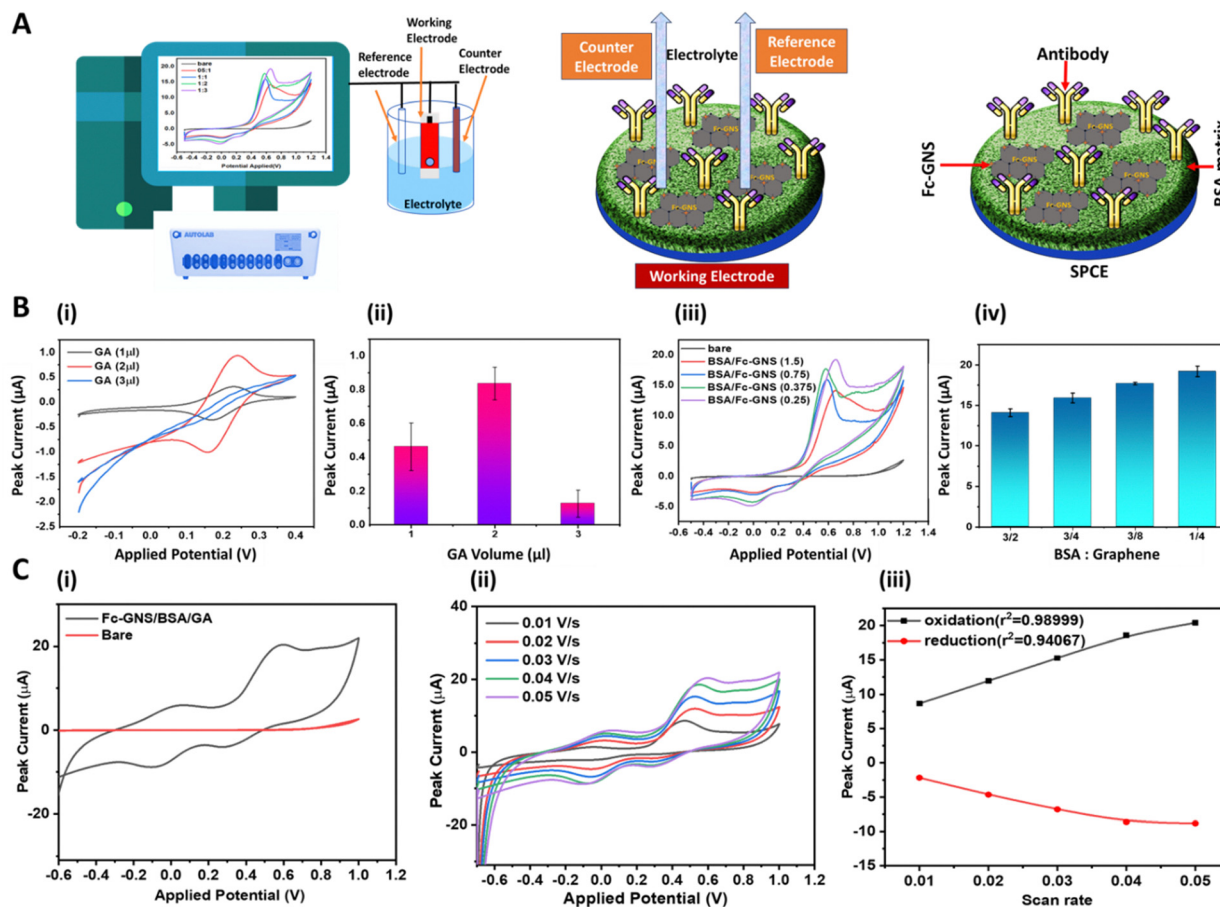


Fig. 4 (A) Schematic depicting the electrochemical setup used to characterize the nanocomposite coating and for immunosensing. (B) (i) CV of BSA/GA coating for different volumes of GA in 5 mM  $\text{Fe}(\text{CN})_6^{3-}/\text{Fe}(\text{CN})_6^{4-}$  and (ii) extracted average peak current values from CV plot to bar graph. (iii) CV of Fc-GNS/BSA/GA coating for different BSA/Fc-GNS concentration ratios in 0.2 M PBS and (iv) extracted average peak current values from CV plot to bar graph. (C) (i) CV of the bare and Fc-GNS/BSA/GA modified SPCE in 0.2 M PBS. (ii) CV of the Fc-GNS/BSA/GA modified SPCE at different scan rates and (iii) extracted oxidation and reduction peak current graphed against the square root of the scan rate.

We selected the BSA/Fc-GNS ratio of 0.375 to synthesize the optimized nanocomposite coating due to its improved charge transfer and enhanced stability.

Finally, we conducted further electrochemical testing to investigate the charge transfer and redox properties of the optimized nanocomposite modified SPCE. The presence of the BSA matrix serves to passivate the electrode surface and prevent biofouling, while effective charge transfer between the ions in solution and the electrode is facilitated by the Fc-GNS. To delve deeper into this hypothesis, we performed CV using the SPCE/Fc-GNS/BSA/GA as the working electrode in a 0.2 M PBS solution at various scan rates, ranging from 0.01 to 0.05  $\text{V s}^{-1}$ , and the resulting voltammograms are presented in Fig. 4C(ii). It was observed that increasing the scan rate led to a linear increase in the peak current values, as highlighted by the linear fit of the oxidation peak current and reduction peak current in relation to the square root of the scan rate, as shown in Fig. 4C(iii). This observation underscores the potential of the Fc-GNS to establish an embedded redox system, highlighting its efficacy in promoting electrochemical biosensing without the need for an external redox mediator.

### 3.4. Anti-fouling performance and immunosensing feasibility

To guarantee the reliability of detection in complex biological fluids, we performed thorough evaluations to assess the effectiveness of the nanocomposite coating in preventing biofouling. This involved incubating the nanocomposite modified SPCE in complex solutions like 1% BSA, artificial urine, and human serum. The uncoated SPCE exhibited a substantial 88% reduction in the normalized peak current variation after a 7-day exposure to artificial urine as shown in Fig. 5A. Consequently, we decided to dismiss further investigations in 1% BSA and serum. In stark contrast, the SPCE/Fc-GNS/BSA/GA demonstrated only a marginal decrease of approximately 16% in the normalized peak current variation after one month of incubation. This compelling outcome highlights the exceptional ability of the nanocomposite coating to resist biofouling which can be primarily attributed to two critical factors: (i) size exclusion: The extensive porosity through efficient crosslinking of BSA using GA, which essentially functions as a sieve, effectively prevents interferences from reaching the electrode surface. (ii) Charge repulsion: the BSA matrix, with an isoelectric point of 4.7, promotes electrostatic repulsion at

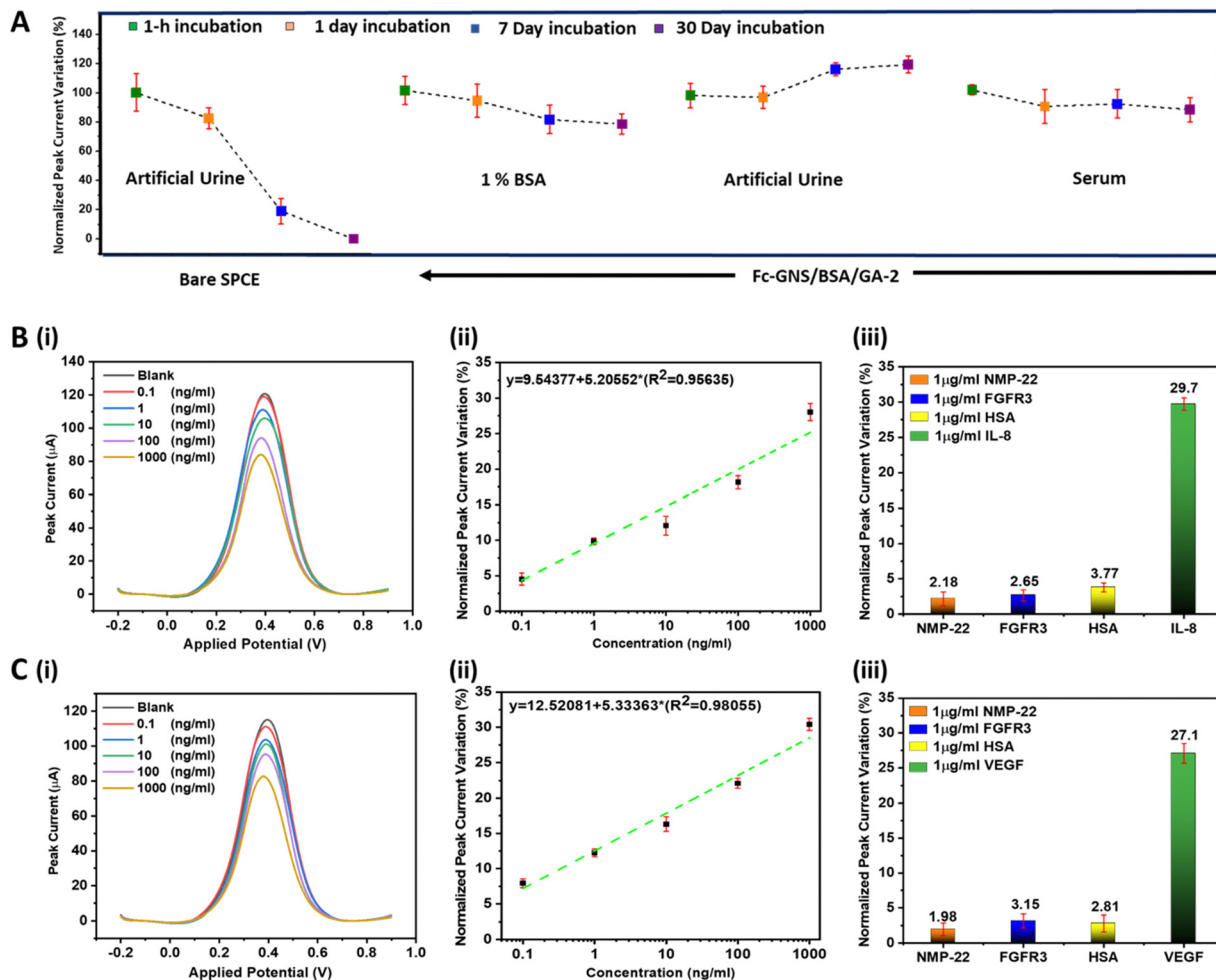


Fig. 5 (A) Antifouling capability of the nanocomposite coated SPCE as compared to the bare SPCE following exposure to various complex fluids for a duration of up to one month. (B) (i) DPV response for different IL-8 concentrations. (ii) Normalized peak current variation (%) extracted from DPV responses for different IL-8 concentrations (iii) specificity test against interfering proteins and comparison with IL-8. (C) (i) DPV response for different VEGF concentrations. (ii) Normalized peak current variation (%) extracted from DPV responses for different VEGF concentrations (iii) specificity test against interfering proteins and comparison with VEGF.

physiological pH which deters soluble proteins from adhering to the surface.

We used the SPCE/Fc-GNS/BSA/GA to develop proof-of-concept immunosensors for the detection of protein biomarkers linked to bladder cancer, specifically IL-8 and VEGF. Following the successful conjugation of the corresponding antibodies through EDC/NHS chemistry, we employed the resulting SPCE/Fc-GNS/BSA/GA/Antibody as the working electrode to directly detect these biomarkers in artificial urine samples. The artificial urine was spiked with different concentrations of the antigen, ranging from  $0.1 \text{ ng mL}^{-1}$  to  $1000 \text{ ng mL}^{-1}$ . To ensure the accuracy and reliability of our results, each antigen concentration was analysed using five separate immunosensors. Subsequently, we extracted the normalized peak current variation from the resulting DPV plots, which is represented as  $\Delta I/I_0\%$ , where  $\Delta I = I$  after (immunosensing)  $- I_0$  (after antibody immobilization). This approach was chosen to effectively express how the immunosensor responds to changes in antigen concentration, as illustrated in Fig. 5B and C. The developed immunosensors

demonstrated high sensitivity for IL-8 and VEGF, with a detection range of  $0.1\text{--}1000 \text{ ng mL}^{-1}$  and calculated LOD of  $41 \text{ pg mL}^{-1}$  and  $67 \text{ pg mL}^{-1}$ , respectively ( $\text{LOD} = 3.3 \sigma/\text{Slope}$ , where  $\sigma$  represents the standard deviation of the regression line). Finally, we conducted a thorough examination of the immunosensors to assess their specificity against interfering proteins commonly found in the urine of bladder cancer patients, such as FGFR3, NMP-22, and HSA. The results revealed that the immunosensors exhibited minimal normalized peak current variation when exposed to  $1 \text{ } \mu\text{g mL}^{-1}$  of these interferents, thus highlighting feasibility for specific detection directly in complex biological fluids.

## 4. Conclusion

In conclusion, this study has made significant strides in addressing a pressing need in the field of electrochemical affinity biosensing in complex biological fluids. The developed 3D nanocomposite coating offers a range of vital functionalities,

including the ability to facilitate oriented covalent conjugation of biorecognition elements, eliminate biofouling and perform mediator-free biosensing directly in complex biological fluids. Notably, the coating demonstrated exceptional antifouling properties even after prolonged exposure to complex fluids such as artificial urine and untreated human serum which is a testament to its suitability for real-world applications. The practicality and effectiveness of this coating were further validated through proof-of-concept feasibility studies, specifically in the electrochemical immunosensing of bladder cancer protein biomarkers IL-8 and VEGF. The achievement of remarkable limits of detection, along with a broad sensing range and high specificity against interferents, showcase the immense potential of this multifunctional coating. This universal electrode coating holds great promise for advancing the field of multiplexed electrochemical biosensing across a wide spectrum of biomarkers found in biological fluids. Ultimately, it opens the door to the development of reliable POCT for a diverse range of medical conditions with the potential to greatly impact healthcare and improve patient lives worldwide.

## Conflicts of interest

There are no conflicts to declare.

## Acknowledgements

The authors would like to thank the Ministry of Science and Technology, Taiwan, for financially supporting this research under Contract no. 111-2222-E-029-001-MY3.

## References

- V. Vanova, K. Mitrevska, V. Milosavljevic, D. Hynek, L. Richtera and V. Adam, Peptide-based electrochemical biosensors utilized for protein detection, *Biosens. Bioelectron.*, 2021, **180**, 113087.
- A. Sanati, M. Jalali, K. Raeissi, F. Karimzadeh, M. Kharaziha and S. S. Mahshid, *et al.*, A review on recent advancements in electrochemical biosensing using carbonaceous nanomaterials, *Microchim. Acta*, 2019, **186**, 1–22.
- N. J. Ronkainen, H. B. Halsall and W. R. Heineman, Electrochemical biosensors, *Chem. Soc. Rev.*, 2010, **39**, 1747–1763.
- J. Sabaté del Río, O. Y. Henry, P. Jolly and D. E. Ingber, An antifouling coating that enables affinity-based electrochemical biosensing in complex biological fluids, *Nat. Nanotechnol.*, 2019, **14**, 1143–1149.
- D. H. Lee, W.-Y. Lee and J. Kim, Introducing Nanoscale Electrochemistry in Small-Molecule Detection for Tackling Existing Limitations of Affinity-Based Label-Free Biosensing Applications, *J. Am. Chem. Soc.*, 2023, **145**, 17767–17778.
- R. K. R. Kumar, A. Kumar, M. O. Shaikh, C.-Y. Liao and C.-H. Chuang, Enzymeless electrochemical biosensor platform utilizing Cu<sub>2</sub>O-Au nanohybrids for point-of-care creatinine testing in complex biological fluids, *Sens. Actuators, B*, 2024, **399**, 134787.
- R. Li, Y. Wen, F. Wang and P. He, Recent advances in immunoassays and biosensors for mycotoxins detection in feedstuffs and foods, *J. Anim. Sci. Biotechnol.*, 2021, **12**, 1–19.
- B. Van Dorst, J. Mehta, K. Bekaert, E. Rouah-Martin, W. De Coen and P. Dubruel, *et al.*, Recent advances in recognition elements of food and environmental biosensors: A review, *Biosens. Bioelectron.*, 2010, **26**, 1178–1194.
- D. Chan, J. C. Chien, E. Axpe, L. Blankemeier, S. W. Baker and S. Swaminathan, *et al.*, Combinatorial polyacrylamide hydrogels for preventing biofouling on implantable biosensors, *Adv. Mater.*, 2022, **34**, 2109764.
- J. Tu, R. M. Torrente-Rodríguez, M. Wang and W. Gao, The era of digital health: A review of portable and wearable affinity biosensors, *Adv. Funct. Mater.*, 2020, **30**, 1906713.
- L. Farzin, M. Shamsipur, L. Samandari and S. Sheibani, Advances in the design of nanomaterial-based electrochemical affinity and enzymatic biosensors for metabolic biomarkers: A review, *Microchim. Acta*, 2018, **185**, 1–25.
- S. Fortunati, F. Pedrini, E. Del Grosso, L. Baranda Pellejero and A. Bertucci, Design of Specific Nucleic Acid-Based Biosensors for Protein Binding Activity, *Analysis Sensing*, 2022, **2**, e202200037.
- D. Sadighbayan, K. Sadighbayan, M. R. Tohid-Kia, A. Y. Khosroushahi and M. Hasanzadeh, Development of electrochemical biosensors for tumor marker determination towards cancer diagnosis: Recent progress, *TrAC, Trends Anal. Chem.*, 2019, **118**, 73–88.
- S. Zhao, Y. Zhang, S. Ding, J. Fan, Z. Luo and K. Liu, *et al.*, A highly sensitive label-free electrochemical immunosensor based on AuNPs-PtNPs-MOFs for nuclear matrix protein 22 analysis in urine sample, *J. Electroanal. Chem.*, 2019, **834**, 33–42.
- H. Zhang and B. L. Miller, Immunosensor-based label-free and multiplex detection of influenza viruses: State of the art, *Biosens. Bioelectron.*, 2019, **141**, 111476.
- R. R. Kumar, A. Kumar, C.-H. Chuang and M. O. Shaikh, Recent advances and emerging trends in cancer biomarker detection technologies, *Ind. Eng. Chem. Res.*, 2023, **62**, 5691–5713.
- M. Patel, M. Agrawal and A. Srivastava, Signal amplification strategies in electrochemical biosensors via antibody immobilization and nanomaterial-based transducers, *Mater. Adv.*, 2022, **3**, 8864–8885.
- R. Rakesh Kumar, M. O. Shaikh, A. Kumar, C.-H. Liu and C.-H. Chuang, Zwitterion-functionalized cuprous oxide nanoparticles for highly specific and enzymeless electrochemical creatinine biosensing in human serum, *ACS Appl. Nano Mater.*, 2023, **6**, 2083–2094.
- Y. Jiang and J. Wu, Recent development in chitosan nanocomposites for surface-based biosensor applications, *Electrophoresis*, 2019, **40**, 2084–2097.
- M. A. Ali, G. F. Zhang, C. Hu, B. Yuan, S. Jahan and G. D. Kitsios, *et al.*, Ultrarapid and ultrasensitive detection of SARS-CoV-2 antibodies in COVID-19 patients via a 3D-printed

- nanomaterial-based biosensing platform, *J. Med. Virol.*, 2022, **94**, 5808–5826.
- 21 A. S. Tanak, B. Jagannath, Y. Tamrakar, S. Muthukumar and S. Prasad, Non-faradaic electrochemical impedimetric profiling of procalcitonin and C-reactive protein as a dual marker biosensor for early sepsis detection, *Anal. Chim. Acta: X*, 2019, **3**, 100029.
  - 22 X. Wang, Z. Zhang, G. Wu, C. Xu, J. Wu and X. Zhang, *et al.*, Applications of electrochemical biosensors based on functional antibody-modified screen-printed electrodes: a review, *Anal. Methods*, 2022, **14**, 7–16.
  - 23 R. R. Kumar, A. Kumar, C.-H. Chuang and M. O. Shaikh, Electrochemical immunosensor utilizing a multifunctional 3D nanocomposite coating with antifouling capability for urinary bladder cancer diagnosis, *Sens. Actuators, B*, 2023, **384**, 133621.
  - 24 J. Bhardwaj, S. Devarakonda, S. Kumar and J. Jang, Development of a paper-based electrochemical immunosensor using an antibody-single walled carbon nanotubes bio-conjugate modified electrode for label-free detection of foodborne pathogens, *Sens. Actuators, B*, 2017, **253**, 115–123.
  - 25 X. Tao, X. Wang, B. Liu and J. Liu, Conjugation of antibodies and aptamers on nanozymes for developing biosensors, *Biosens. Bioelectron.*, 2020, **168**, 112537.
  - 26 L. E. McCrae, W.-T. Ting and M. M. Howlader, Advancing electrochemical biosensors for interleukin-6 detection, *Biosens. Bioelectron.: X*, 2022, 100288.
  - 27 C. Ibañ, M. M. Arshad and S. C. Gopinath, Current advances and future visions on bioelectronic immunosensing for prostate-specific antigen, *Biosens. Bioelectron.*, 2017, **98**, 267–284.
  - 28 M. Mahmoudpour, A. Jouyban, J. Soleymani and M. Rahimi, Rational design of smart nano-platforms based on anti-fouling-nanomaterials toward multifunctional bioanalysis, *Adv. Colloid Interface Sci.*, 2022, **302**, 102637.
  - 29 N. Liu, Z. Xu, A. Morrin and X. Luo, Low fouling strategies for electrochemical biosensors targeting disease biomarkers, *Anal. Methods*, 2019, **11**, 702–711.
  - 30 R. K. Rakesh Kumar, M. O. Shaikh, A. Kumar, C.-H. Liu and C.-H. Chuang, Zwitterion-Functionalized Cuprous Oxide Nanoparticles for Highly Specific and Enzymeless Electrochemical Creatinine Biosensing in Human Serum, *ACS Appl. Nano Mater.*, 2023, **6**, 2083–2094.
  - 31 W. Wang, R. Han, M. Chen and X. Luo, Antifouling Peptide Hydrogel Based Electrochemical Biosensors for Highly Sensitive Detection of Cancer Biomarker HER2 in Human Serum, *Anal. Chem.*, 2021, **93**, 7355–7361.
  - 32 Y. Wang, J. Luo, J. Liu, S. Sun, Y. Xiong and Y. Ma, *et al.*, Label-free microfluidic paper-based electrochemical aptasensor for ultrasensitive and simultaneous multiplexed detection of cancer biomarkers, *Biosens. Bioelectron.*, 2019, **136**, 84–90.
  - 33 R. R. Kumar, M. O. Shaikh and C.-H. Chuang, A review of recent advances in non-enzymatic electrochemical creatinine biosensing, *Anal. Chim. Acta*, 2021, **1183**, 338748.
  - 34 L. Wu and X. Qu, Cancer biomarker detection: recent achievements and challenges, *Chem. Soc. Rev.*, 2015, **44**, 2963–2997.
  - 35 D. Liu, J. Wang, L. Wu, Y. Huang, Y. Zhang and M. Zhu, *et al.*, Trends in miniaturized biosensors for point-of-care testing, *TrAC, Trends Anal. Chem.*, 2020, **122**, 115701.
  - 36 Y. Esmaeili, E. Bidram, A. Zarrabi, A. Amini and C. Cheng, Graphene oxide and its derivatives as promising In-vitro bio-imaging platforms, *Sci. Rep.*, 2020, **10**, 18052.
  - 37 Y. Ji, X. Yang, Z. Ji, L. Zhu, N. Ma and D. Chen, *et al.*, DFT-Calculated IR Spectrum Amide I, II, and III Band Contributions of N-Methylacetamide Fine Components, *ACS Omega*, 2020, **5**, 8572–8578.
  - 38 L. Wang, J. Zhu, H. Yang, F. Wang, Y. Qin and T. Zhao, *et al.*, Fabrication of hierarchical graphene@Fe<sub>3</sub>O<sub>4</sub>@SiO<sub>2</sub>@polyaniline quaternary composite and its improved electrochemical performance, *J. Alloys Compd.*, 2015, **634**, 232–238.
  - 39 D. Dabur, N. Sharma and H.-F. Wu, “Synergistic effect” based novel and ultrasensitive approach for the detection of serotonin using DEM-modulated bimetallic nanosheets, *J. Mater. Chem. B*, 2023, **11**, 6044–6052.
  - 40 P. M. Hallam, M. Gómez-Mingot, D. K. Kampouris and C. E. Banks, Facile synthetic fabrication of iron oxide particles and novel hydrogen superoxide supercapacitors, *RSC Adv.*, 2012, **2**, 6672–6679.
  - 41 T. Yamashita and P. Hayes, Analysis of XPS spectra of Fe<sup>2+</sup> and Fe<sup>3+</sup> ions in oxide materials, *Appl. Surf. Sci.*, 2008, **254**, 2441–2449.
  - 42 M. Sakurai, P. Koley and M. Aono, Morphological Change of Molecular Assemblies through On-Surface Chemical Reaction, *J. Phys. Chem. C*, 2019, **123**, 29679–29685.